Article

Not peer-reviewed version

Five-Axis Finish Milling Machining for an Inconel 718 Alloy Monolithic Blisk

Ming-Hsu Tsai * , Teng-Hui Chen , Jeng-Nan Lee , Tai-Lin Hsu , Dong-Ke Huang

Posted Date: 2 April 2024

doi: 10.20944/preprints202404.0113.v1

Keywords: Monolithic blisk; Five-axis machining; Machining parameter; Tool wear

 doi:10.20944/preprints202404.0113.v1

Article

Five-Axis Finish Milling Machining for an Inconel 718 Alloy Monolithic Blisk

Ming-Hsu Tsai [1,2,*], Teng-Hui Chen [1,2], Jeng-Nan Lee [1,2], Tai-Lin Hsu [2] and Dong-Ke Huang [2]

[1] Department of Mechanical Engineering, Cheng Shiu University, Kaohsiung 833301, Taiwan
[2] Institute of Mechatronics Engineering, Cheng Shiu University, Kaohsiung 833301, Taiwan
* Correspondence: k0635@gcloud.csu.edu.tw; Tel.: +886-7-7358800 #3321

Abstract: Blisks subjected to rough machining for channel creation must undergo finishing processes, and such processes must achieve the required tolerance limits. A high-quality surface finish and predictable long tool life are critical for the finish milling of blisks. Accordingly, the aim of this study was to optimize parameters for the finish machining of an Inconel 718 alloy monolithic blisk. Ball-cone mills were used to machine the blade surface at a constant depth. A sensory tool holder was used to collect cutting force signals during machining, and a digital microscope was used to examine tool wear. The surface texture measuring instrument was used to measure blisk blade surface roughness to evaluate processing quality. This study manipulated two cutting parameters, namely cutting speed and feed per tooth, and investigated their effects. The relationship between cutting conditions and machining efficiency was analyzed. According to the experimental results, we identified a set of optimal parameters for marginal tool wear and fast cutting speeds and then estimated the corresponding tool life by using the derived parameters.

Keywords: monolithic blisk; five-axis machining; machining parameter; tool wear

1. Introduction

A monolithic blisk is a critical component of an aircraft engine (aero engine). In contrast to the traditional fan design, in which multiple removable blades are assembled on an individual disk, the design of a blisk entails integrating the blades of the blisk with the disk. This design can reduce weight, improve stability during high-speed revolutions, and improve the performance of engines. Moreover, the design obviates the necessity of assembling the blades and the disk during the production process, which improves manufacturing efficiency. Blisks can be manufactured using various methods; the most common method involves machining from solid material by using machine tools. However, because a blisk has a complex geometry and requires high temperatures and durability, it must have excellent mechanical properties. The requirements for material selection, processing environment, and precision in the manufacturing process are strict. Blisks are usually made from difficult-to-cut materials such as titanium and nickel-based alloys and require the use of multiaxis machine tools and complex toolpath planning by using suitable tools and cutting parameters.

Inconel 718 has been used frequently in blisk materials because of its superior mechanical properties. However, the machinability of Inconel 718 is relatively low owing to its extreme performance. This thermal-resistant alloy exhibits high strength and tends to exhibit strain hardening even at high temperatures, resulting in high cutting forces and extreme temperatures during machining. Traditional carbide tools wear quickly during machining, especially uncoated tungsten carbide inserts employed under dry conditions [1]. Research has focused on improving the machining efficiency of Inconel 718 through the use of tool coatings, use of coolants, and optimization of cutting parameters [2]. Liquid coolants, also known as cutting fluids, are used to cool the tool and workpiece by removing the heat generated during machining. Pereira et al. proposed the use of external MQL lubrication (CryoMQL) with CO2 as an internal coolant for the cryogenic cooling of Inconel 718 during milling [3]. This ambient cooling method was demonstrated to engender increased tool life

 doi:10.20944/preprints202404.0113.v1

[4]. Kursuncu et al. conducted cryogenic heat treatment on cemented carbide tools to increase their wear resistance and thus improve their cutting performance [5].

Scholars have extensively discussed the effect of cutting conditions, including the tool material and geometry, feed rates, and radial depth of cuts, on tool life [6]. Different cutting methods with various cutting parameters and machining strategies have been proposed for controlling tool wear [7]. Moreover, a study introduced a laser preheating–assisted system and ultrasonically assisted system for optimizing cutting parameters and improving cutting performance [8]. The computer-aided engineering (CAE) software was also used to predict the deformations and stresses of the spindle and cutting tools under external loads to evaluate the rationality of cutting conditions [9,10].

The first step of blisk machining entails rough milling, followed by the establishment of a boundary contour on the free surface of the blade [11] and then the control of the tool axis and cutting path to remove the groove material [12]. Traditional flank mills or barrel cutters are often used for machining [13]. In rough machining, efficiency is essential. Studies have presented a plunge milling strategy or four-axis cycloid path for material removal to improve efficiency [14,15]. Although most studies on blisk machining have discussed roughing processes [16], the blisk must be finished ultimately to achieve the required tolerance limits. A high-quality surfacbladenish and predictable, long tool life are critical considerations in blisk milling. Selecting the optimal machining parameters to obtain the desired surface quality and tool life is the most critical task in blisk finishing.

The aim of the present study was to optimize parameters for the finish machining of Inconel 718 alloy monolithic blisk blades. AlTiN-coated ball cone mills were used to machine the surfaces of the blades at a constant depth. The study also investigated the effects of two manipulated cutting parameters: cutting speed and feed per tooth. Cutting force signals during the machining process were collected using a sensory tool holder, and tool wear was observed under a digital microscope. The relationship between cutting conditions and machining efficiency was analyzed. The study results can serve as a reference in the optimization of parameters for the finish machining of blisk blades.

2. Machining of Blisk Blades

Figure 1 depicts a computer-aided design (CAD) model and solid model of a typical monolithic blisk. A nickel-based alloy was subjected to rough machining and grooving processes to produce the blisk; subsequently, the finishing path of the blade was planned according to the shape of the machined blisk by using the impeller module in NX software, as illustrated in Figure 2. The driving method was blade finishing milling. In the multi-axis machining of NX, in order to better control the inclination angle of the tool axis, we can set the lead angle and tilt angle according to the direction of the tool path. Previous studies disclosed that when the inclination angle is 25° in machining, the workpiece will have better surface roughness [17]. After selecting the blade surface, we set the tilt angle of the tool to 0.2° and set the minimum lead angle to −30°. A negative lead angle value indicates that the tool is tilted backward relative to the tool path direction. The tool axis was automatically determined by the NX program. After the toolpath was completed, VERICUT—a virtual cutting program—was used for verification to avoid the interference in the toolpath and prevent collisions. Figure 3 presents the relationship between the tool axis and the blade surface in VERICUT.

 doi:10.20944/preprints202404.0113.v1

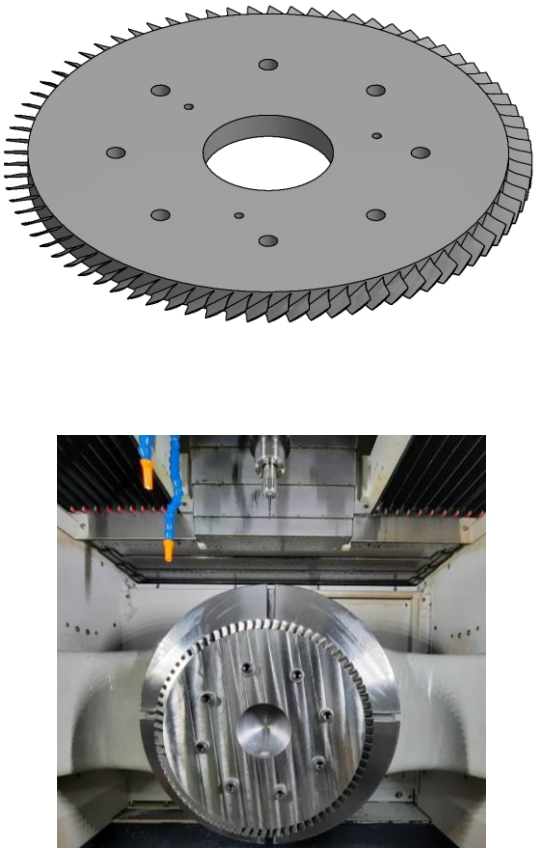

Figure 1. CAD Model and Solid Model of Monolithic Blisk.

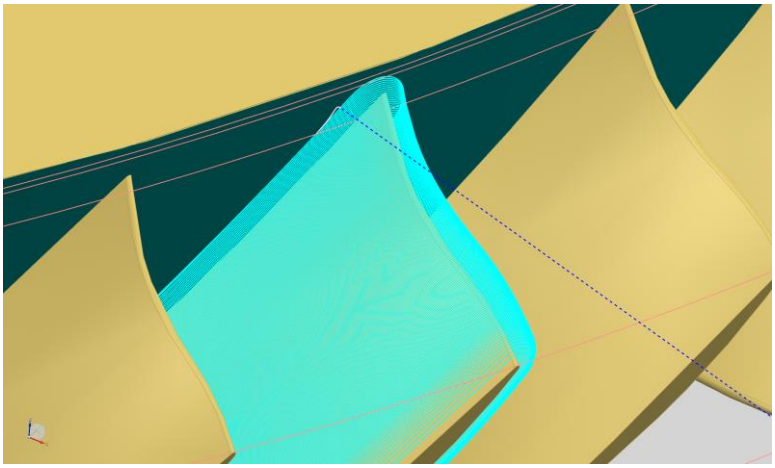

Figure 2. Blade Finishing Tool Path on NX.

Preprints.org (www.preprints.org) | NOT PEER-REVIEWED | Posted: 2 April 2024 doi:10.20944/preprints202404.0113.v1

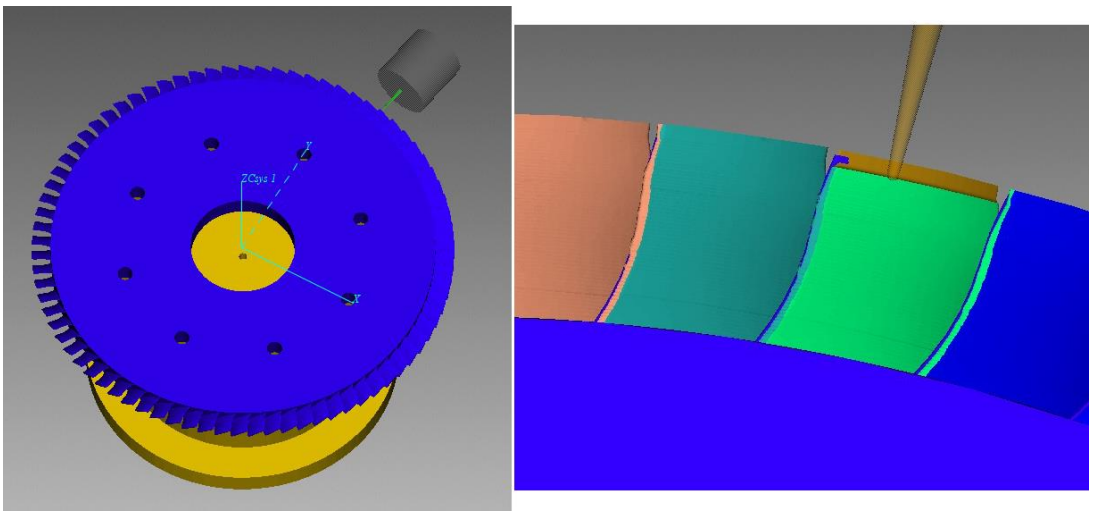

Figure 3. Tool Axis in VERICUT.

2.1. Blisk Machining Parameters

The outer diameter of the blisk was 364 mm, the outer diameter of the hub was 331.5 mm, the length of the blade was 16.25 mm, the thinnest part of the blade was approximately 0.23 mm, the thickest part of the blade was approximately 1.59 mm, the groove width was approximately 6.46 mm, and the number of blades was 78. The primary dimensions are presented in Figure 4.

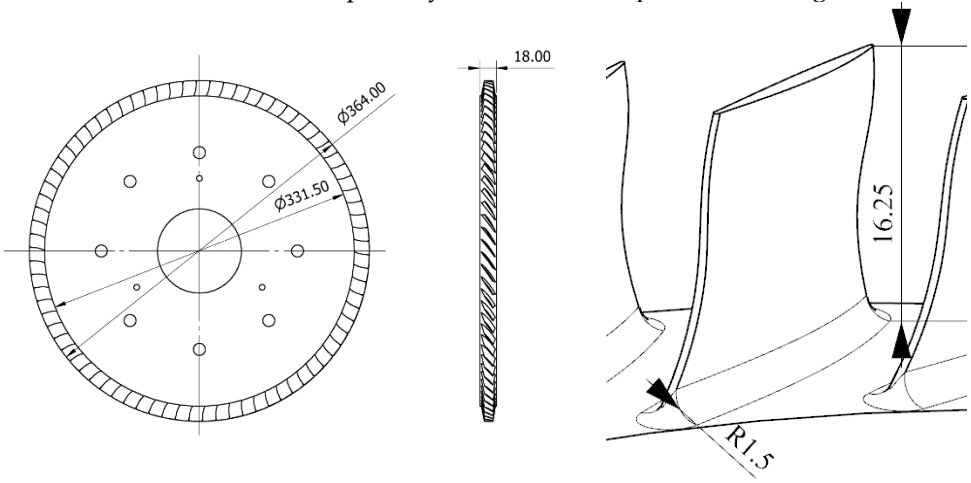

Figure 4. Dimensions of Monolithic Blisk (unit: mm).

2.2. Material

Inconel 718 has high strength and oxidation/corrosion resistance at elevated temperatures, rendering it suitable for high kinetic–energy and corrosion-resistant environments in the aerospace industry. Inconel 718 is primarily composed of nickel and chromium. Nickel can improve heat resistance and corrosion resistance, and chromium can improve oxidation resistance and sulfur resistance. Table 1 lists the mechanical properties of Inconel 718, which were provided by the material supplier Xitron Innovation [18].

Table 1. Mechanical Properties of Inconel 718.

Property	Values
Density (g/cm3)	8.19
Poisson's Ratio	0.29
Young's Modulus (GPa)	200
Ultimate Stress (MPa)	860

 doi:10.20944/preprints202404.0113.v1

Yield Stress (MPa)	551
Elongation (%)	51.7
Hardness (HRB)	97.7
Thermal Conductivity (W/m.K)	11.2

2.3. Experimental Equipment

2.3.1. Machine Tool

The milling machine was a five-axis machining center CT-630 (Tongtai, Kaohsiung, Taiwan) equipped with a Siemens 840Dsl CNC controller.

2.3.2. Cutting Tools

The material of a cutting tool considerably influences the machining of Inconel 718 alloy blisks. The tool must have high thermal hardness, good ductility, high wear resistance, and high impact resistance. In this study, a tapered ball-nose end mill (Jen Wu Cheng Shun Turning Tools, Kaohsiung, Taiwan) was used for machining, as displayed in Figure 5. Several studies on the machining of nickel-base alloys had showed that TiAlN coated tools have better tool life in high speed milling than other coatings, such as TiN and TiCN [19]. Therefore, this study used TiAlN-coated. The specifications of the tool are presented in Table 2 [20].

Figure 5. Tapered Ball Nose End Mill.

Table 2. Specification of Tapered Ball Nose End Mill.

Property/Composition	Values
Shank Diameter (mm)	6
Tool Nose Ridus (mm)	1.5
Over length (mm)	75
Cutting length (mm)	20
Single Side Angel (degree)	3
Flutes	2
Material	Tungsten Carbide
Coating	AlTiN

2.3.3. Sensory Tool Holder

A sensory tool holder (pro-micron, Kaufbeuren, Germany) was used to measure cutting force signals [21]. The sensory tool holder collected the axial cutting force, cutting torque, and x–y bending moment during the finish machining of the blisk blades and wirelessly sent the collected data to a computer. Because the tool axis was set to side milling during the cutting process, the bending moment was selected as the primary observation parameter. Polar diagrams of the bending moment in the x–y direction were used to observe the force in real time [22]. The specifications of the sensory tool holder are presented in Table 3.

Table 3. Specification of Sensory Tool Holder.

Property	Values
Measuring frequency (Hz)	2500
Maximum allowable speed (rpm)	18000
Operating temperature (°C)	0–50
Collet size	ER20

 doi:10.20944/preprints202404.0113.v1

Spindle taper	BBT-40
Total length (mm)	155

2.3.4. Digital Microscope

A digital microscope (VHX900F, Keyence, Osaka, Japan) with depth-of-field synthesis and multiple illumination functions was used to examine the milling cutters during the experiments. The microscope was used to examine the wear of the cutting edge and the side edge after machining. The magnification of the microscope ranges from 20× to 1000×; we set the magnification to 100× to examine the tools.

3. Finish Machining Strategy and Method

The machining strategy first involved rough machining on the blank and grooving using a torus milling cutter with D5R0.5. The thickest part of the blade was machined to a thickness of 2.18 mm. To ensure the surface quality, a ball-end mill with R2.0 was used for semifinish machining. Processed the thickest part of the blade to 1.78 mm with the machining allowance set to 0.1 mm. Finally, the tapered ball-nose end mill was used for finishing to the required dimensions 1.59 mm. The machining process is displayed in Figure 6. During the machining process, we set different parameters for the cutting speed and feed per tooth to observe the cutting bending moment and tool wear.

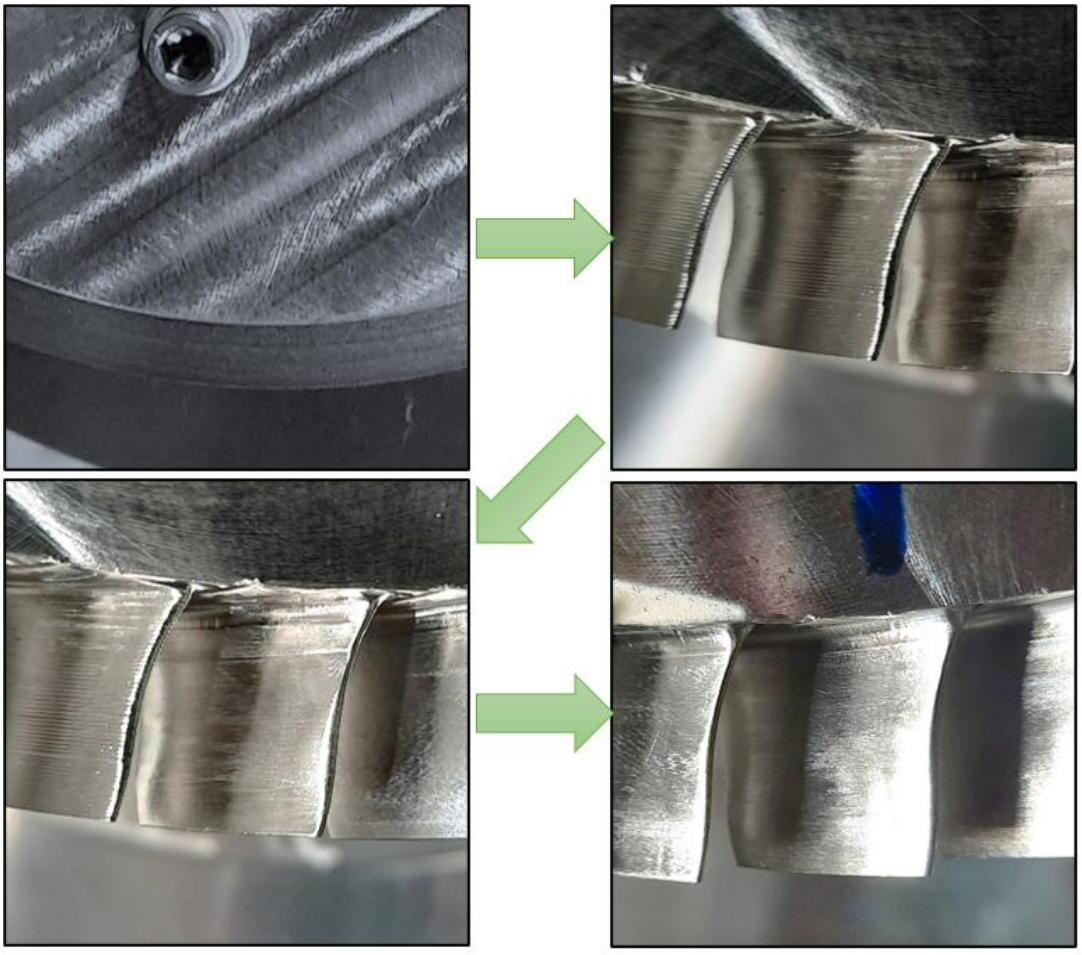

Figure 6. Blank → Roughing → Semi-Finishing → Finishing.

 doi:10.20944/preprints202404.0113.v1

3.1. Cutting Speed

3.1.1. Processing Conditions and Parameters

It was reported that feed has no significant effect on carbide cutter milling Inconel 718 [17]. Nevertheless, cutting speed Vc is related closely to cutting force and tool wear. An appropriate range of cutting speed for side milling has been proposed in the literature. Hence, in our experiments, the depth of cut Ap and feed per tooth Fz were fixed, and different cutting speeds were set (ranging from 26 to 96 m/min). The effective cutting speed Ve during the cutting process is very important. It is calculated based on the effective diameter De, as shown in Figure 7 [23].

$$De = Dc*\sin(\varphi+\theta), \quad (1)$$

$$\cos\theta = 1-2*Ap/Dc, \quad (2)$$

Where Dc is the ball nose diameter. φ is the inclination angle of the tool. Because the lead angle is set to -30° in the NX program, the maximum tool inclination angle is 30°. The maximum effective diameter De can be calculated to be 2.115mm. When the cutting depth is tiny, the effective cutting speed is much lower than the setting speed, and the tool cutting conditions will be lower than its application range. Therefore, this study recalculated the effective cutting speed Ve.

$$Ve = Vc*De/Dc, \quad (3)$$

Thus, eight experiments were performed. The effective cutting speeds after recalculation were listed in Table 4. Each experiment was a complete process in which a new tool was used for blade cutting. In Experiment 7, the cutting speed was originally set to 86 m/min, and the spindle speed was set to 9125 RPM, which resonated with the machine. Therefore, the cutting speed was increased to 91 m/min in this experiment. Under the fixed feed per tooth, an increase in the cutting speed also engendered an increase in feed, which reduced the time required for processing.

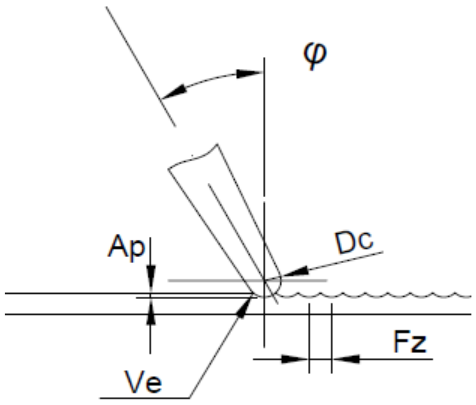

Figure 7. The effective cutting speed Ve for inclined milling.

Table 4. Machining parameters I.

	Cutting Speed Vc (m/min)	Effective Cutting Speed Ve (m/min)	Feed per Tooth Fz (mm/tooth)	Depth of Cut Ap (mm)	Time (min:sec)
Exp. 1	26	19.33	0.05	0.05	56:25
Exp. 2	36	25.38	0.05	0.05	40:53
Exp. 3	46	32.43	0.05	0.05	32:08
Exp. 4	56	39.48	0.05	0.05	26:26
Exp. 5	66	46.53	0.05	0.05	22:30
Exp. 6	76	53.59	0.05	0.05	19:43

 doi:10.20944/preprints202404.0113.v1

Exp. 7	91	64.16	0.05	0.05	16:48
Exp. 8	96	67.69	0.05	0.05	16:06

3.1.2. Cutting Signal Capture and Analysis

During the machining process, cutting force signals were captured by the sensory tool holder. Because the toolpath involved side milling using a side rake, the tool was mainly subjected to lateral forces. The bending moment was thus used as the basis for evaluating the cutting condition. The toolpath progressed from the periphery of the blade to the hub on a layer-by-layer basis along the blade surface, as illustrated in Figure 2. The bending moment signals captured in each experiment were recorded on the basis of the cutting layer, as shown in Figure 8. The bending moments recorded in Experiments 4, 7, and 8 increased, and those captured in the other experiments remained relatively stable.

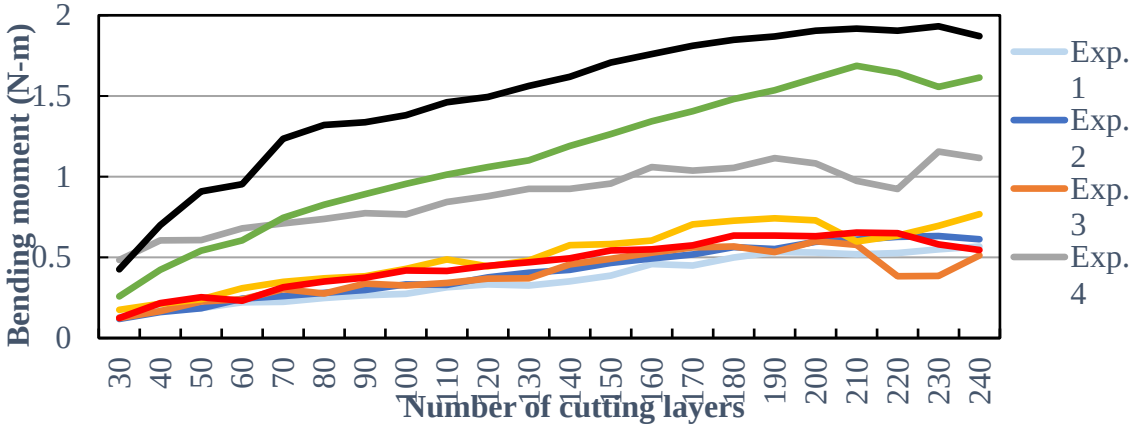

Figure 8. Bending Moments at Different Cutting Speeds.

3.1.3. Tool Wear and Cutting Moment

The captured bending moment signals during processing in the x direction and y direction were plotted on the x- and y-axes, respectively, and a polar diagram of the bending moment signals was generated, as displayed in Figure 9. The size and distribution of the plots on the polar diagram were examined to determine the cutting force and damage to the tool die. According to the distribution of the plots, Experiments 1–3 exhibited the most concentrated and uniform distributions, indicating that the force in the cutting process was average and stable. The graphs of Experiments 7 and 8 were relatively scattered and revealed that the cutting edge was 2. The data revealed that the bending moment increased. Tool wear was observed under a digital microscope with a magnification of 100×, as depicted in Figure 10. Because of the setting of the tool axis (Figure 3), the contact area between the tool and the blade was on the side cutting edge of the front end of the tool. The most severe wear occurred on the flank of the side edge. The tool flank in Experiments 4, 7, and 8 demonstrated severe wear, which corresponded to an increase in bending moment (Figure 7).

 doi:10.20944/preprints202404.0113.v1

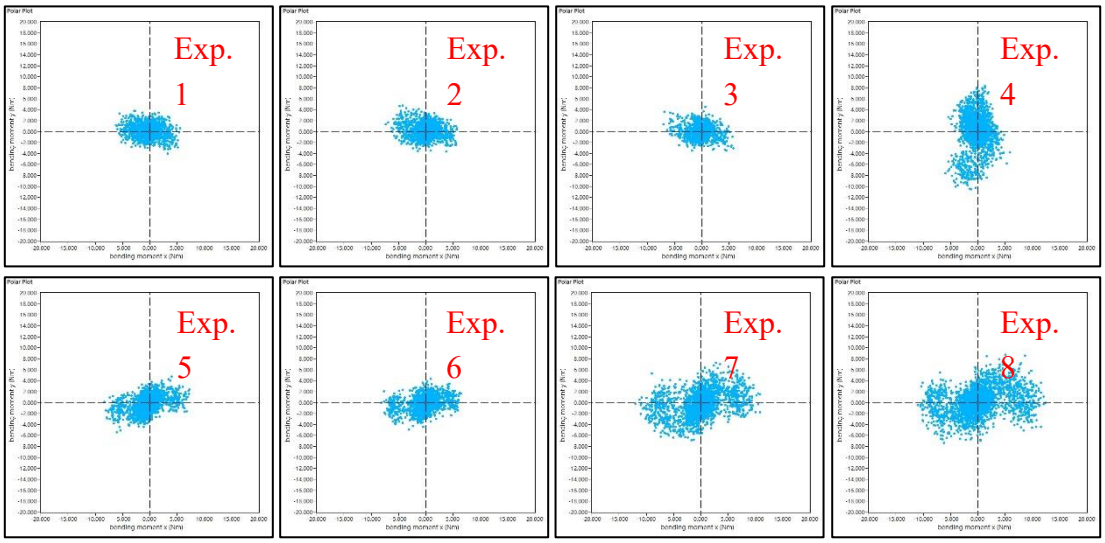

Figure 9. Bending Moment in Polar Coordinates at Different Cutting Speeds.

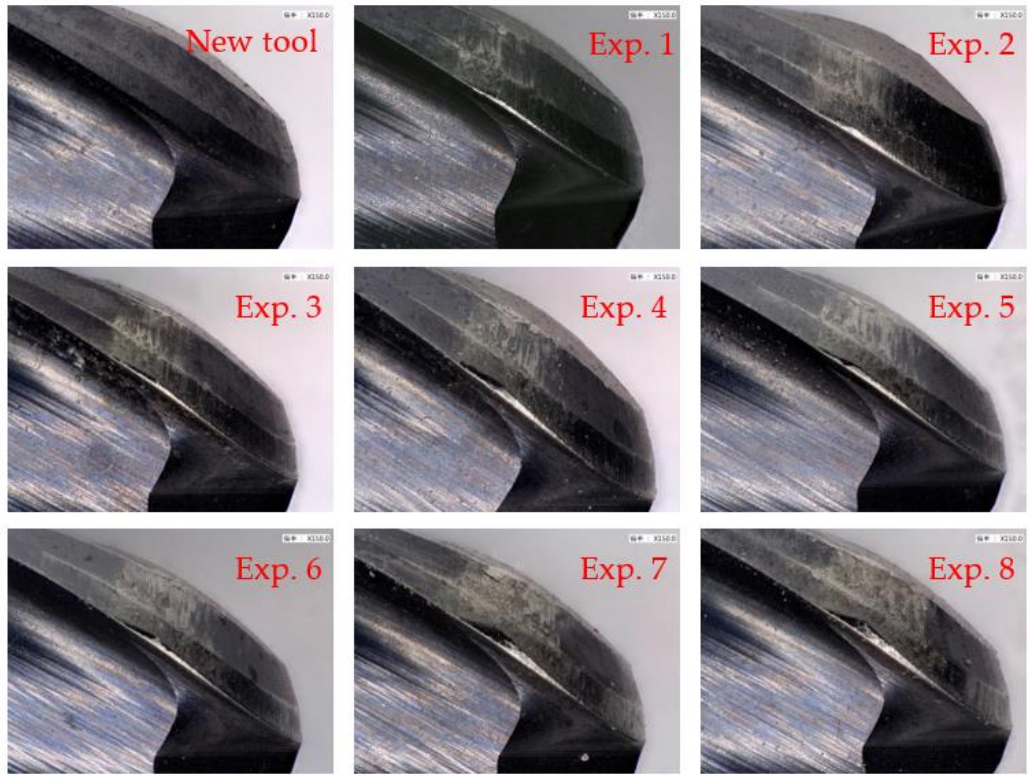

Figure 10. This is a figure. Schemes follow the same formatting.

3.2. *Feed Per Tooth*

3.2.1. Processing Conditions and Parameters

According to the experimental results regarding cutting speeds, we also considered tool wear and machining efficiency. Cutting speeds of 66 and 76 m/min were selected as the reference, and the feed per tooth was adjusted. The machining parameters were determined and are presented in Table 5. A new tool was used for each experiment.

 doi:10.20944/preprints202404.0113.v1

Table 5. Machining parameters II.

	Cutting Speed Vc (m/min)	Effective Cutting Speed Ve (m/min)	Feed per Tooth Fz (mm/tooth)	Depth of Cut Ap (mm)	Time (min:sec)
Exp. 9	66	46.53	0.05	0.05	22:30
Exp. 10	66	46.53	0.075	0.05	16:36
Exp. 11	66	46.53	0.1	0.05	13:02
Exp. 12	76	53.59	0.05	0.05	19:43
Exp. 13	76	53.59	0.075	0.05	14:09
Exp. 14	76	53.59	0.1	0.05	12:14

3.2.2. Cutting Signal Capture and Analysis

As presented in Figure 11, Experiments 9 and 12 yielded lower bending moment curves than did the other experiments. When the feed per tooth was set to 0.05 mm, less cutting force was observed. The cutting forces at a feed per tooth of 0.1 and 0.075 mm were similar.

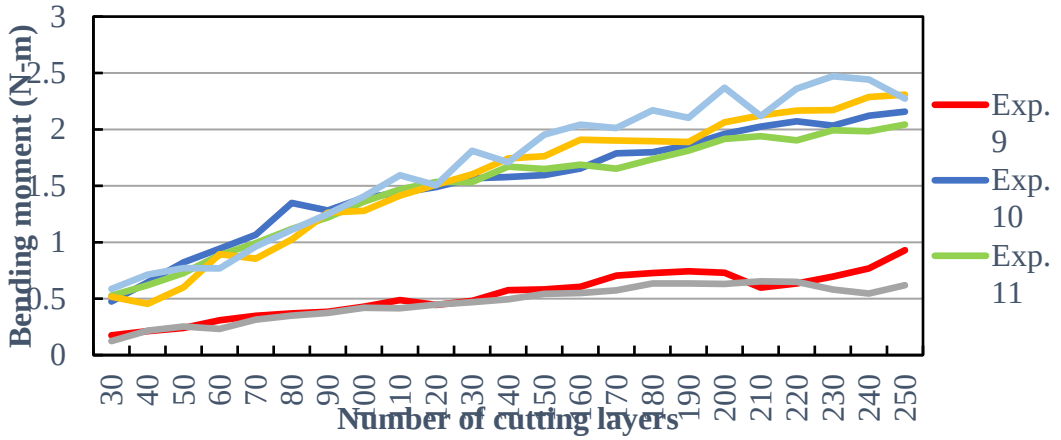

Figure 11. Bending Moments at Different Feeds Per Tooth.

3.2.3. Tool Wear and Cutting Moment

According to the polar diagram of the bending moment, the distributions observed for Experiments 9 and 12 were more concentrated than those observed for the other experiments (Figure 12). The other diagrams revealed a relatively large cutting force, and the tool may break at dense points. The tool exhibited various degrees of wear under magnification, as illustrated in Figure 13. Experiments 9 and 12 yielded relatively low wear, which may be due to their small bending moment.

Preprints.org (www.preprints.org) | NOT PEER-REVIEWED | Posted: 2 April 2024 doi:10.20944/preprints202404.0113.v1

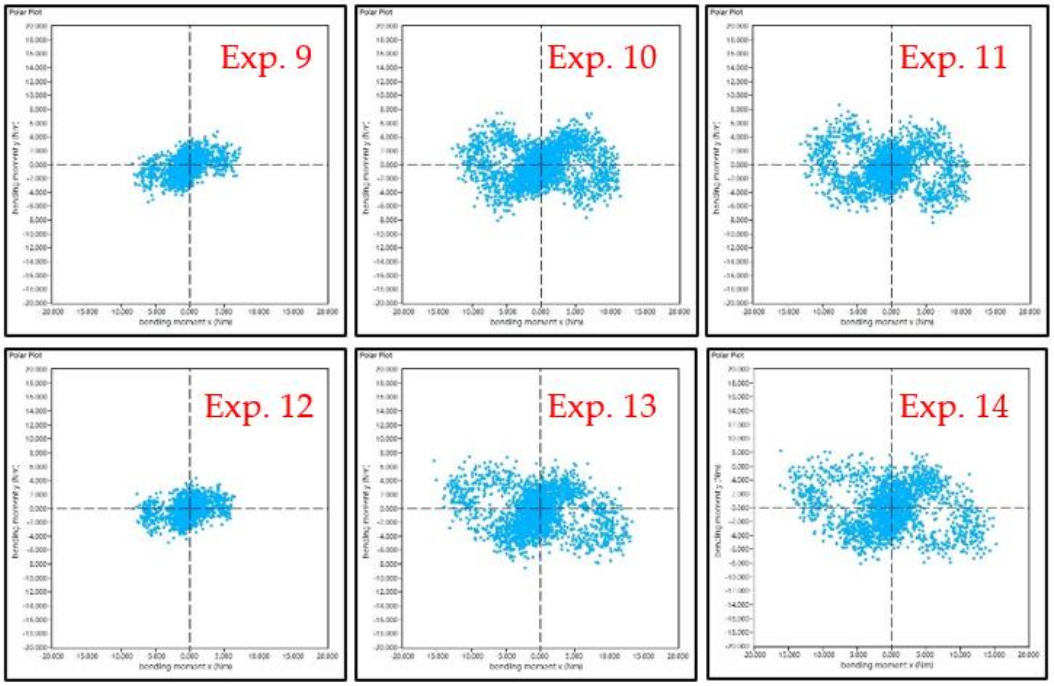

Figure 12. Polar Coordinates of Bending Moment at Different Feeds Per Tooth.

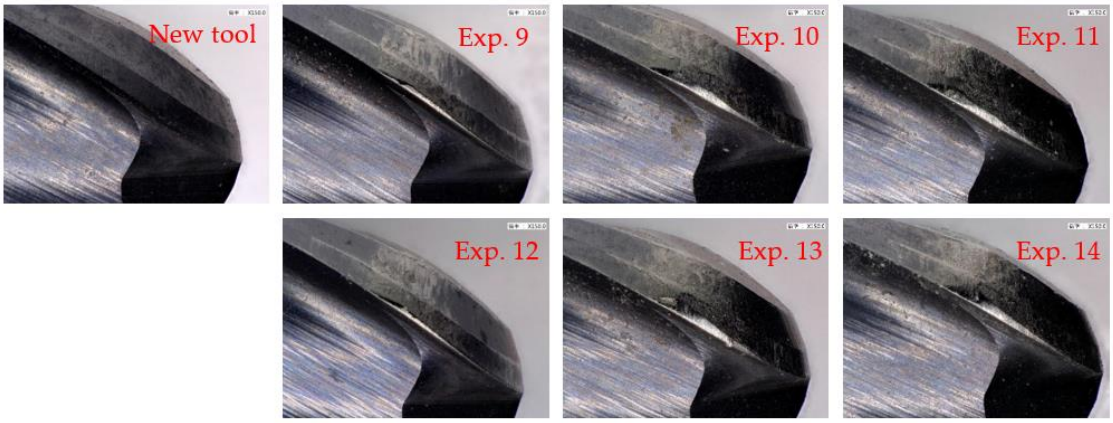

Figure 13. Flank Wear at Different Feeds Per Tooth.

4. Tool Life Test

Through basic cutting experiments, we determined the relationship between cutting parameters, bending moments, and tool wear. The experimental results could be used to evaluate machining efficiency and surface roughness requirements. For mechanical efficiency considerations, this study expected the blade surface roughness to reach a satin finish, which means the roughness requirement is RZ6.3. We measured the finished surface roughness, as shown in Figure 14. According to the measurement results, we explored reasonable machining parameters that could be used to test the tool life.

Preprints.org (www.preprints.org) | NOT PEER-REVIEWED | Posted: 2 April 2024 doi:10.20944/preprints202404.0113.v1

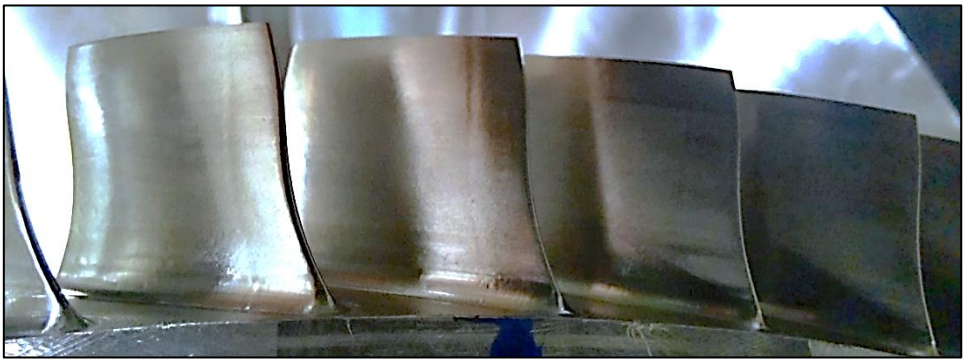

Figure 14. Finished Blade Surface.

4.1. Assessment of Surface Roughness

Currently, two methods are widely used in the aerospace industry to measure surface roughness: contact and noncontact. We used the noncontact method by portable surface texture measuring instrument for online measurement during processing. The instrument was HANDYSURF+35 (TOKYO SEIMITSU, Tokyo, Japan) and its resolution can reach 0.0007μm. Each blade was measured three times to get the average. Non-contact 3D white light interferometer microscope Opt-scope (TOKYO SEIMITSU, Tokyo, Japan) with a high vertical resolution of 0.01nm was used for offline measurement. We compared the results of the two measurement methods, as shown in Figure 15. The results revealed that all processing results in Experiments 1–14 fulfilled the roughness requirements.

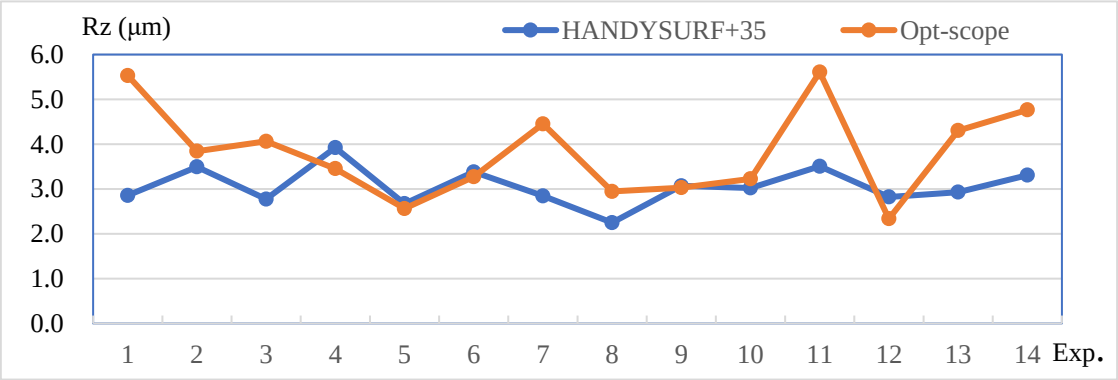

Figure 15. Surface roughness measurement results.

4.2. Repetitive Experiments

The basic cutting experiments revealed optimal machining parameters yielding small and stable cutting forces, which helped improve the surface quality of the blade. However, considering processing efficiency, one can adjust the machining parameters within an acceptable surface quality to shorten the machining time. We selected the parameters of Experiment 11 and performed repeated experiments by using the same tool 12 times (Table 6) for tool life assessment.

Table 6. Machining parameters III.

	Cutting Speed Vc (m/min)	Effective Cutting Speed Ve (m/min)	Feed per Tooth Fz (mm/tooth)	Depth of Cut Ap (mm)	Time (min:sec)
Exp. 15~26	66	46.53	0.1	0.05	13:02

 doi:10.20944/preprints202404.0113.v1

4.3. Bending Moment and Tool Wear

The cutting force increased steadily as the experiment progressed, as shown in Figure 16. The bending moment demonstrated a step jump after Experiment 23. We assessed magnified images of the tool and detected a crack on the flank of the tool after Experiment 23 (Figure 17); this crack was indicated by the increase in bending moment. On the basis of the evaluation results, we determined that the tool life was approximately 8 blades under the selected surface quality and efficiency parameters.

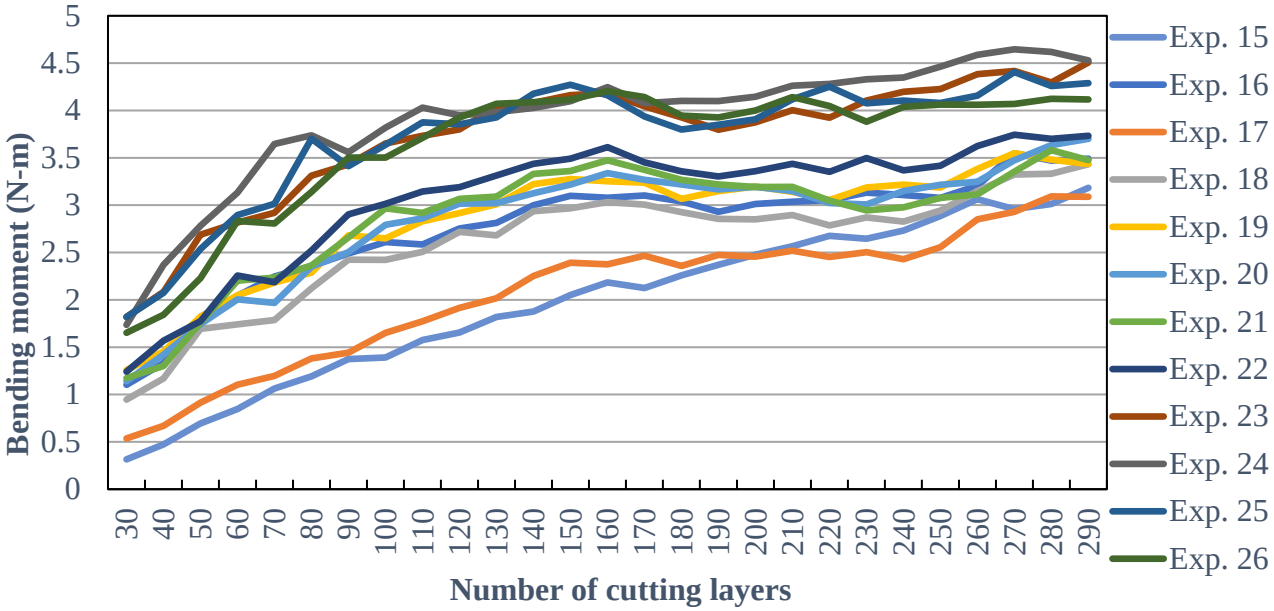

Figure 16. Bending Moments in Repeated Experiments.

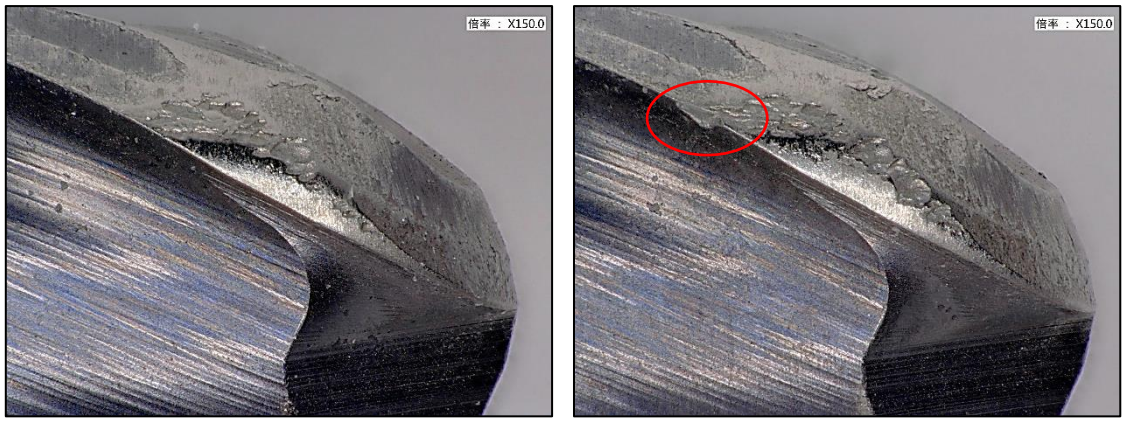

Figure 17. Flank Wear After Experiments 22 (Left) and 23 (Right).

5. Conclusions

In this study, we conducted basic cutting and tool life experiments to analyze cutting conditions in blisk finishing processes. Force signals collected by a sensory tool holder directly indicated the cutting forces, and the influence of machining parameters on the cutting forces was nonlinear; this could thus help us select efficient parameters. The bending moment diagram also accurately indicated tool wear, which could help us estimate the time required to change the tool. On the basis of our findings, we drew the following conclusions:

(1) A cutting speed between 66 and 76 m/min (effective cutting speed between 46 and 53 m/min) can provide a relatively low cutting force, which can short the machining time and maintain surface quality.

 doi:10.20944/preprints202404.0113.v1

(2) A feed per tooth of 0.05 mm can provide a relatively low cutting force, and a feed per tooth of 0.075 and 0.1 mm can provide relatively high cutting forces with similar values.

(3) A cutting speed of 66 mm/min (effective cutting speed of 46 m/min) and feed per tooth of 0.1 mm can provide the most stable cutting force and the highest processing efficiency.

(4) Under the aforementioned conditions, a tapered ball-nose end mill can process a total of 8 blades.

Author Contributions: Conceptualization, M.-H.T. and J.-N.L.; methodology, M.-H.T.; software, T.-L.H. and D.-K.H.; validation, T.-H.C.; formal analysis, M.-H.T.; investigation, T.-H.C.; resources, J.-N.L.; data curation, D.-K.H.; writing—original draft preparation, D.-K.H.; writing—review and editing, M.-H.T.; supervision, T.-H.C.; project administration, M.-H.T.; funding acquisition, J.-N.L. All authors have read and agreed to the published version of the manuscript.

Funding: This research received no external funding.

Institutional Review Board Statement: Not applicable.

Informed Consent Statement: Not applicable.

Data Availability Statement: Not applicable.

Acknowledgments: This manuscript was edited by Wallace Academic Editing.

Conflicts of Interest: The authors declare no conflict of interest.

References

1. Alauddin M.; El Baradie M.A.; Hashmi M.S.J. Tool-life testing in the end milling of Inconel 718. *J. Mater. Process. Technol*. **1995**, 55(3-4), 321-330.
2. Kuo C.P.; Su S.C. ; Chen S.H. Tool life and surface integrity when milling Inconel 718 with coated cemented carbide tools. *J. Chin. Inst. Chem. Eng.* **2010**, 33(6), 915-922.
3. Pereira O.; Urbikain G.; Rodríguez A.; Fernández-Valdivielso A.; Calleja A.; Ayesta I.; López de Lacalle L.N. Internal cryolubrication approach for Inconel 718 milling. *Procedia. Manuf.* **2017**, 13, 89-93.
4. Pereira O.; Celayab A.; Urbikaín G.; Rodríguez A.; Fernández-Valdivielso A.; López de Lacalle L.N. CO2 cryogenic milling of Inconel 718: cutting forces and tool wear. *J. Mater. Res. technol*. **2020**, 9(4), 8459–8468.
5. Kurşuncu B.; ÇAY V.V. Effect of deep cryogenic treatment on cutting performance in Inconel 718 milling. *IENSC* **2019**, 948-953.
6. Krain H.R.; Sharman A.R.C.; Ridgway K. Optimisation of tool life and productivity when end milling Inconel 718TM. *J. Mater. Process. Technol.* **2007**, 189, 153-161.
7. Szablewski P.; Dobrowolski T.; Chwalczuk T. Optimization of Inconel 718 milling strategies. *Mechanik* **2019**, 92(12), 824-826.
8. Lin S.Y.; Yang B.H. Experimental Study of Cutting Performance for Inconel 718 Milling by Various Assisted Machining Techniques. *Solid State Phenom.* **2019**. 294. 129-134.
9. Hong C.C.; Chang C.L.; Ou N.R.; Lin C.Y. CAE Analysis of Primary Shaft Systems in Great Five-Axis Turning-Milling Complex CNC Machine. *Proc. eng. technol. innov.* **2019**, 12, 01–08.
10. Hong C.C.; Chang C.L.; Huang C.C.; Yang C.C.; Lin C.Y. CAE Analysis of Secondary Shaft Systems in Great Five-axis Turning-Milling Complex CNC Machine. *Adv. technol. innov.* **2017**, 3, 43–50.
11. Hu C.G.; Zhang D.H.; Ren J.X.; Yang L. Research on the 5-axis Machining of Blisk. *Mater. Sci. Forum* **2006**. 532-533. 612-615.
12. Huang J.C.; Liu X.L.; Yue C.X.; Cheng Y.N.; Zhang H. Tool Path Planning of 5-Axis Finishing Milling Machining for Closed Blisk. *Mater. Sci. Forum* **2012**, 723, 153–8.
13. Lu Y.A.; Ding Y.; Wang C.Y.; Zhu L.M. Tool path generation for five-axis machining of blisks with barrel cutters. *Int. J. Prod. Res.* **2019**, 57(5), 1300-1314.
14. Shan C.W.; Zhang D.H.; Ren J.X.; Hu C.G. Research on the Plunge Milling Techniques for Open Blisks. *Mater. Sci. Forum* **2006**, 532–533, 193–196.
15. Luo M.; Hah C.; Hafeez H.M. Four-axis trochoidal toolpath planning for rough milling of aero-engine blisks. *Chin. J. Aeronaut.* **2019**, 32(8), 2009-2016,
16. Chen T.H.; Lee J.N.; Tsai M.H.; Shie M.J.; Lin C.Y. Optimization of milling parameters based on five-axis machining for centrifugal impeller with titanium alloy. *J. Phys.: Conf. Ser.* **2022**, 2345, 012019.
17. Liao Y.S.; Lin H.M.; Wang J.H. Behaviors of end milling Inconel 718 superalloy by cemented carbide tools. *J. Mater. Process. Technol.* **2008**, 201(1-3), 460-465.
18. Xitron Innovation Co. Ltd. https://www.ixitron.com/ (accessed October 2022).
19. Sharman A.; Dewes, R.C.; Aspinwall D.K. Tool life when high speed ball nose end milling Inconel 718. *J. Achiev. Mater.* **2001,** 118(1–3), 29–35.

 doi:10.20944/preprints202404.0113.v1

20. Jen Wu Cheng Shun Turning Tool CO. LTD. http://www.jsk-tools.com.tw/ (accessed October 2022).
21. Lu Z.; Wang M.; Dai W. Machined surface quality monitoring using a wireless sensory tool holder in the machining process. *Sensors*, **2019**, 19(8), 1847.
22. Tsai M.H.; Lee J.N.; Shie M.J.; Deng M.H. Intelligent Performance Prediction of Flank Milling of Ti6Al4V Using Sensory Tool Holder. *Sens. Mater*. **2022**, 34(8), 3241-3253.
23. Daymi A.; Boujelbene M.; Linares J.M.; Bayraktar E.; Amara, A. Influence of workpiece inclination angle on the surface roughness in ball end milling of the titanium alloy Ti-6Al-4V. *J. Achiev. Mater. Manuf. Eng.* **2009**, 35(1), 79–86.